NANO LETTERS
Cite This: Nano Lett. 2018, 18, 798−804
Letter
pubs.acs.org/NanoLett

Roles of Mo Surface Dopants in Enhancing the ORR Performance of Octahedral PtNi Nanoparticles

Qingying Jia,[*,†] Zipeng Zhao,[‡,§] Liang Cao,[∥] Jingkun Li,[†] Shraboni Ghoshal,[†] Veronica Davies,[†] Eli Stavitski,[⊥] Klaus Attenkofer,[⊥] Zeyan Liu,[‡,§] Mufan Li,[§,#] Xiangfeng Duan,[§,#] Sanjeev Mukerjee,[†] Tim Mueller,[*,∥] and Yu Huang[*,‡,§]

[†]Department of Chemistry and Chemical Biology, Northeastern University, Boston, Massachusetts 02115, United States
[‡]Department of Materials Science and Engineering, University of California, Los Angeles, California 90095, United States
[§]California NanoSystems Institute (CNSI), University of California, Los Angeles, California 90095, United States
[∥]Department of Materials Science and Engineering, Johns Hopkins University, Baltimore, Maryland 21218, United States
[⊥]National Synchrotron Light Source II, Brookhaven National Laboratory, Upton, New York 11973, United States
[#]Department of Chemistry and Biochemistry, University of California, Los Angeles, California 90095, United States

Supporting Information

ABSTRACT: Doping with a transition metal was recently shown to greatly boost the activity and durability of PtNi/C octahedral nanoparticles (NPs) for the oxygen reduction reaction (ORR), but its specific roles remain unclear. By combining electrochemistry, *ex situ* and *in situ* spectroscopic techniques, density functional theory calculations, and a newly developed kinetic Monte Carlo model, we showed that Mo atoms are preferentially located on the vertex and edge sites of Mo−PtNi/C in the form of oxides, which are stable within the wide potential window of the electrochemical cycle. These surface Mo oxides stabilize adjacent Pt sites, hereby stabilizing the octahedral shape enriched with (111) facets, and lead to increased concentration of Ni in subsurface layers where they are protected against acid dissolution. Consequently, the favorable $Pt_3Ni(111)$ structure for the ORR is stabilized on the surface of PtNi/C NPs in acid against voltage cycling. Significantly, the unusual potential-dependent oxygen coverage trend on Mo-doped PtNi/C NPs as revealed by the surface-sensitive $\Delta\mu$ analysis suggests that the Mo dopants may also improve the ORR kinetics by modifying the coordination environments of Pt atoms on the surface. Our studies point out a possible way to stabilize the favorable shape and composition established on conceptual catalytic models in practical nanoscale catalysts.

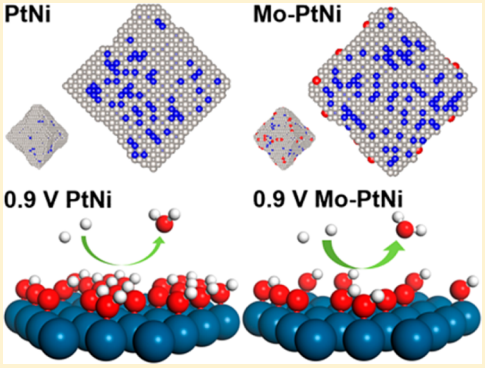

KEYWORDS: *ORR, Mo−PtNi, acid dissolution, in situ XAS, kinetic Monte Carlo, density functional theory*

Discovery of new materials often inspires new theories, and *vice versa*. This constitutes a general spiral process of material science. In 2007, Markovic et al. discovered the concept of the $Pt_3Ni(111)$ catalytic system with a record-high activity toward the oxygen reduction reaction (ORR).[1] The record activity of $Pt_3Ni(111)$ originates from the combination of the pure Pt(111) surface with the Ni underneath that lowers the *d*-band center of the Pt(111) surface via strain and electronic effects, given that $Pt_3Ni(111)$ is far more active than Pt(111) (without Ni), as well as $Pt_3Ni(110)$ and $Pt_3Ni(100)$ (without the (111) facet).[1,2] Since then, substantial efforts have been dedicated to developing nanoscale PtM/C catalysts (M represents a transition metal like Co, Ni, Cu, etc.) with the surface structure and composition mimicking those of $Pt_3Ni(111)$ to pursue high ORR performance in practical devices.[3−7] The (111) facet enrichment can be realized by constructing nanoclusters with the octahedral shape,[7,8] and the incorporation of the Ni in the core can be achieved by alloying and dealloying Pt with Ni.[5,6,9−11] The resultant octahedral PtNi/C nanoparticles (NPs) indeed exhibit exceptional ORR activity.[7,8] However, the favorable $Pt_3Ni(111)$ morphology is inherently unstable in the highly acidic and corrosive environments at the fuel cell cathode, under which Ni continuously leaches out from the NPs resulting in the attenuation of the Ni-induced strain and ligand effects;[5,9,12] and the under-coordinated Pt sites relocate onto the (111) facet via migration and dissolution/redeposition processes, leading to the loss of the octahedral shape and the enriched (111) facet.[5,13,14] As a result, the ORR activity decreases markedly upon long-term fuel cell operation.[15,16] Therefore, stabilizing favorable shape and composition under *operando*

Received: September 18, 2017
Revised: November 26, 2017
Published: December 22, 2017

DOI: 10.1021/acs.nanolett.7b04007
Nano Lett. 2018, 18, 798−804

conditions constitutes a grand challenge in developing active and durable catalysts.

Recently, Huang et al.[3] reported a group of transition-metal-doped PtNi/C octahedral catalysts (denoted as M−PtNi/C) with exceptional activity and durability toward the ORR. In particular, the nanoscale Mo−Pt_3Ni/C catalyst exhibited a specific activity approaching that of the $Pt_3Ni(111)$ model catalyst.[1] Cao and Mueller[3,17] suggested based on computations that surface Mo oxides help retain the shape and composition of octahedral PtNi NPs by stabilizing low-coordinated Pt sites and reducing equilibrium surface Ni composition, thereby enhancing the durability. The high durability of M−PtNi/C was also experimentally confirmed by Strasser's group[18] on Rh-doped octahedral PtNi/C NPs. They attributed the enhanced stability to the Rh-induced stabilization of the octahedral shape via the suppression of surface Pt migration rather than Ni dissolution. Most recently, Alonso-Vante et al. reported that both the ORR activity and stability of the PtCu nanoparticles were greatly improved by the doped Mo in the forms of oxidation resistant alloyed Mo-doped atoms.[19] While surface dopants have emerged as a general design approach to enhance the performance of nanocatalysts, the specific roles of these surface dopants in boosting the activity and retaining the desired surface morphology of PtM/C catalysts remain largely elusive. Besides the indirect roles of Mo in retaining the $Pt_3Ni(111)$ like surface on nanocatalysts, the possibility of Mo dopants directly modifying ORR kinetics has never been explored, which is an important topic from both fundamental and practical perspectives.

Herein, we aim to fill the knowledge gaps by coupling synthetic efforts with experimental studies (including *ex situ* and *in situ* electrochemical and synchrotron-based X-ray absorption spectroscopic (XAS) studies), and theoretical studies (including density functional theory (DFT)[20] calculations, Metropolis Monte Carlo,[21] and kinetic Monte Carlo (KMC) simulations[22,23] using a cluster expansion[17,24,25]) on PtNi/C NPs with and without surface-doped Mo as model catalysts. We provide experimental and computational evidence for the presence of Mo oxides (Mo^{4+}/Mo^{6+}) on the surface of Mo−PtNi/C octahedral NPs within the entire fuel cell potential cycling range. In addition, we unravel the roles of the surface-doped Mo in promoting kinetics by stabilizing a $Pt_3Ni(111)$-like surface structure of octahedral PtNi/C NPs in acid against voltage cycling, as well as in modifying the coordination environments of Pt atoms on the surface. These new findings provide a structural and mechanistic basis for the high ORR performance of the M−PtNi/C catalysts recently developed by Huang et al.,[3] and in a broad context partly constitute the fundamental principles of the surface decoration strategy for optimization and stabilization of the surface morphology of nanoclusters.

The PtNi/C and Mo−PtNi/C octahedral NPs were synthesized using improved approaches based on those previously reported[3] (details are provided in the Supporting Information). Both PtNi/C and Mo−PtNi/C octahedra have an average size (edge length) around 5.5 nm, and their X-ray diffraction (XRD) patterns indicate single Pt−Ni alloy phase (Figure S1). With similar Pt loading (12.2 $\mu g/cm^2$ Pt on electrode), a smaller overpotential and higher mass and specific activities were observed in Mo−PtNi/C on a rotating disk electrode (RDE) (Figure 1A, Figure S2), after 30 cycles of cyclic voltammetry (CV) activation in nitrogen saturated 0.1 M $HClO_4$ (scan rate 100 mV/s, 0.05 to 1.1 V, all potentials are versus reversible hydrogen electrode (RHE) in this work), suggesting better kinetics based on the shift of ORR polarization curve toward the thermodynamic equilibrium ORR potential (1.23 V). In addition, accelerated stability tests showed Mo−PtNi/C with higher stability compared to PtNi/C (Figure S3), consistent with previously reported results.[3,18,19]

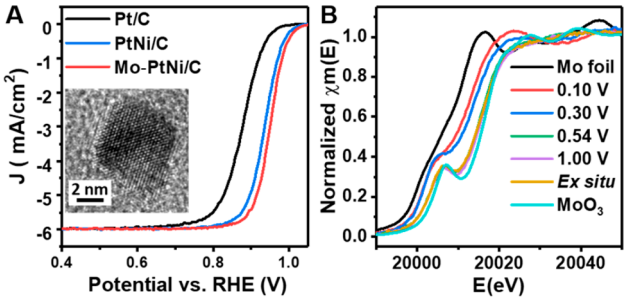

Figure 1. (A) ORR polarization curves of Mo−PtNi/C, PtNi/C, and Pt/C catalysts recorded at room temperature in an O_2-saturated 0.1 M $HClO_4$ aqueous solution with a sweep rate of 20 mV/s and a rotation rate of 1600 rpm. Insert is high resolution transmission electron microscopy image of Mo-PtNi/C. (B) The Mo K-edge XANES spectra collected on Mo foil, MoO_3, and Mo−PtNi/C dry electrode *ex situ* and in an O_2-purged 0.1 M $HClO_4$ electrolyte as a function of applied potentials.

In situ and *ex situ* electrochemical and synchrotron-based X-ray absorption spectroscopic (XAS) studies, as well as computations were performed to reveal the promoting roles of the surface Mo dopants. The compositions of the PtNi/C and Mo−PtNi/C were first characterized by energy dispersive spectroscopy (EDS) and inductively coupled plasma atomic emission spectroscopy (ICP-AES) (Table 1). The slight difference in the Pt/Ni ratio between PtNi/C and Mo−PtNi/C can be attributed to the extended reaction time due to the second step growth in Mo−PtNi/C. After 30 cycles of CV activation, we found that the Pt/Ni ratio of the PtNi/C changed from 72.8/27.2 to 83.4/16.6, corresponding to a loss of ~47% of the total Ni content. In contrast, the Ni loss in Mo−PtNi/C is much less (ca. 18% of total Ni content). The higher Ni retention of Mo−PtNi/C compared with PtNi/C is also directly visible from the EDS line scan comparison (Figure S4). The Mo composition decreases from 1.6% to 0.4% (Table 1) upon the activation. The presence of the surface Mo under *in situ* conditions, and the concomitant suppression of Ni loss upon acid treatment are confirmed by *in situ* XAS as shown next.

Table 1. Composition of the Octahedral PtNi/C and Mo−PtNi/C Samples before and after Activation (Based on EDS and ICP-AES)[a]

sample		atomic ratio (%)		
		Pt	Ni	Mo
octahedral PtNi/C	before activation	72.8	27.2	
	after activation	83.4	16.6	
octahedral Mo−PtNi/C	before activation	70.0	28.6	1.4
	after activation	74.6	25.0	0.4

[a]The activation process: 30 CV cycles in nitrogen saturated 0.1 M $HClO_4$ (scan rate 100 mV/s, 0.05 to 1.1 V vs. RHE).

DOI: 10.1021/acs.nanolett.7b04007
Nano Lett. 2018, 18, 798−804

We characterized these catalysts by synchrotron-based XAS at all the Pt, Ni, and/or Mo edges to explore the atomic structures of PtNi/C and Mo−PtNi/C under both *ex situ* and *in situ* conditions. It was found that the Mo K-edge X-ray absorption near edge structure (XANES) spectra shift toward higher energy with increasing potential until 0.54 V (Figure 1B). The *in situ* XANES remains unchanged with further increased potentials and overlaps the *ex situ* XANES collected on the dry electrode. This shift was previously observed on Pt−Mo/C NPs and related to the Mo^{4+}/Mo^{6+} redox behavior of the Mo surface oxides at 0.45 V.[26] These XAS results also agree well with the previous *ex situ* X-ray photoelectron spectroscopy (XPS) results on the similar Mo−PtNi/C catalyst,[3] which indicates that the Mo in Mo−PtNi/C is mainly in the form of Mo^{6+} and Mo^{4+} states. The presence of the Mo dopants on the surface is likely driven by its reversible redox process potential within the operating potential range.[18] These *in situ* data unambiguously confirm the presence of electrochemically active Mo surface oxides in acid under ORR conditions, which constitutes the prerequisite for justifying the roles of Mo dopants, given that the substantial loss of Mo during the activation process (Table 1) implicates the possibility of complete loss of metal oxides doped via different methods.

The Ni distribution in the Mo−PtNi/C and PtNi/C NPs was investigated by comparing their *ex situ* and *in situ* XAS data collected at the Ni K-edge (Figure 2). The edge step of the Ni

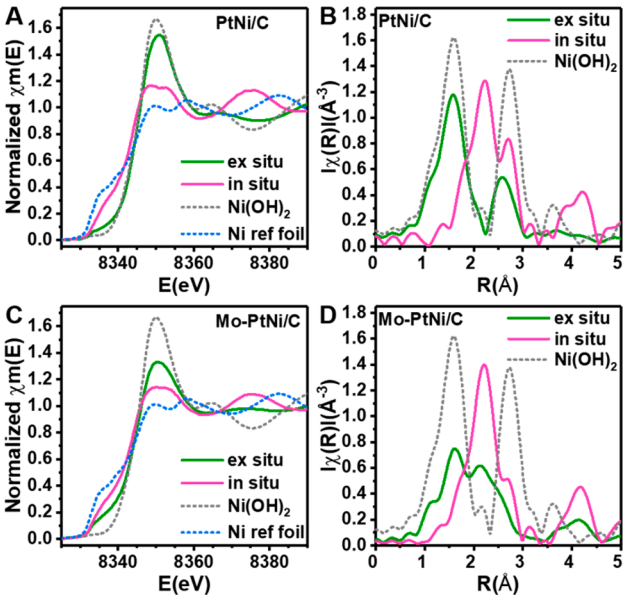

Figure 2. *Ex situ* and *in situ* Ni K-edge XANES (left) and FT-EXAFS (right) spectra of PtNi/C (A,B) and Mo−PtNi/C (C,D), with Ni reference foil and $Ni(OH)_2$ standard. *In situ* data were collected in an O_2-purged 0.1 M $HClO_4$ electrolyte, which did not change with applied potentials.

K-edge XANES of the dry electrode of PtNi/C under *ex situ* conditions drops dramatically under *in situ* electrochemical conditions after CV activation (Figure S5). This indicates a substantial loss of Ni upon the CV activation since the edge step is proportional to the number of absorbing atoms passed by the X-ray beam,[27] consistent with the XPS (Figure S6 and Table S1), EDS, and ICP-AES results (Table 1). The white line intensity of the normalized Ni XANES of the *ex situ* PtNi/C dry electrode approaches that of $Ni(OH)_2$ and is much higher than that of the Ni reference foil (Figure 2A). It reduces drastically under *in situ* conditions in acid and remains unchanged with changing potentials (Figure S7). Correspondingly, the Fourier transform of the extended X-ray absorption fine structure (FT-EXAFS) of the *ex situ* PtNi/C dry electrode closely resembles that of $Ni(OH)_2$ (Figure 2B). It changes dramatically *in situ* with the Ni−O scattering peak around 1.5 Å disappeared (Figure 2B). The *in situ* FT-EXAFS can be well fitted with a Ni−Pt alloy model without including Ni−O scattering paths (Table S2). These results together verify that the Ni in the PtNi/C dry electrode is in the mixed forms of Ni^{x+} and Pt−Ni alloying phase. The Ni^{x+} was located at the surface and dissolved by the acid treatment; whereas the Pt−Ni alloying phase is protected in the core. This configuration is intuitive considering the strong affinity of Ni for oxygen and has been widely observed on PtNi NPs.[9,28−30] The presence of surface Ni species is likely driven by the strong tendency of Ni segregation to the surface in the presence of oxidizing species.[30] These surface Ni species will not contribute to the ORR performance since they will be completely leached out during the activation process. However, the Ni in the core is beneficial for ORR not only because it enhances the utilization of Pt but also improves the specific activity of the surface Pt sites by shortening the Pt−Pt bond distance.[31,32] This so-called strain effect is evidenced by the shorter Pt−Pt bond distance of PtNi/C (2.735 ± 0.004 Å, Table S2) compared to that of Pt/C (2.757 ± 0.003 Å, Table S3) as revealed by the EXAFS fitting, and accounts primarily for the superior ORR activity of PtNi/C to that of Pt/C. The substantial Ni loss of PtNi/C caused by the modest CV activation indicates the poor Ni retention of the conventional PtNi/C catalysts in acidic media, which seriously limits their activity and durability in the cathode of proton exchange membrane fuel cells (PEMFCs).[9,31]

The XAS results obtained on the Mo−PtNi/C catalysts show the similar Ni dissolution occurrence but stark difference in the Ni distribution (Figure 2C,D). The edge step of the Ni K-edge XANES drops from *ex situ* conditions to *in situ* (Figure S8) in Mo−PtNi/C, but the extent is much less compared to that of PtNi/C, consistent with the reduced Ni loss in Mo−PtNi/C upon the CV activation observed by EDS (Table 1) and XPS (Figure S9 and Table S1). The *ex situ* white line intensity of Mo−PtNi/C is lower than that of PtNi/C (Figure 2A,C). This indicates that relatively less Ni is located in the surface of Mo−PtNi/C in the form of Ni^{x+} compared to PtNi/C, in agreement with the XPS deconvolution analysis (Figures S6 and S9).[33] Correspondingly, the *ex situ* FT-EXAFS of Mo−PtNi/C exhibits a suppressed Ni−O scattering peak (~1.5 Å), and clear peaks around 2.1 and 4.2 Å associated with the Pt−Ni alloying phase (Figure 2D). As a result of the acidic dissolution of the surface Ni^{x+}, Mo−PtNi/C contains more Ni in the core than that in PtNi/C under *in situ* conditions, which is confirmed by *in situ* EXAFS fitting of the Ni K-edge and Pt L_3-edge spectra of Mo−PtNi/C and PtNi/C catalysts (Figure S14 and Tables S2−S4). The EXAFS analyses indicate that the local coordination environment of the Ni in PtNi/C (N_{NiPt} = 8.0 ± 0.8; N_{NiNi} = 4.4 ± 1.2) is close to that of the random bulk Pt_3Ni model (N_{NiPt} = 9; N_{NiNi} = 3); whereas the local coordination environment of the Ni in Mo−PtNi/C (N_{NiPt} = 5.6 ± 0.8; N_{NiNi} = 5.8 ± 1.1) is close to that of random bulk Pt_1Ni_1 (N_{NiPt} = 6; N_{NiNi} = 6), verifying higher Ni content in the Mo−PtNi/C NPs.[34] The higher Ni content in the Mo−PtNi/C is also reflected by its shorter Pt−Pt bond distance

DOI: 10.1021/acs.nanolett.7b04007
Nano Lett. 2018, 18, 798−804

(2.724 ± 0.002 Å, Table S4) compared to that of PtNi/C (2.735 ± 0.004 Å, Table S2) as per Vegard's law. These results are consistent with the higher Ni content in Mo−PtNi/C after activation as seen by XPS and EDS (Table 1; Table S1 and Figures S4, S6, and S9). The combined XAS, EDS, and ICP-AES results provide the first experimental evidence that a lower fraction of Ni is presented on the surface of Mo−PtNi/C compared to PtNi/C, resulting partly in less Ni loss during the activation process.

To understand why higher Ni content is observed for Mo−PtNi/C in the presence of surface Mo oxides after CV activation, we have used a cluster expansion[17] trained on DFT calculations to examine the atomic structures of PtNi/C and Mo−PtNi/C before and after activation. Metropolis Monte Carlo simulations[21] (details are provided in sections 3.2 and 3.3 of the Supporting Information) predict that in equilibrium the core of the nanoparticle should form an ordered $L1_2$ phase,[3,17] which is inconsistent with the EXAFS analyses. This suggests that the particles are kinetically trapped in a metastable state. To analyze this state, we have developed a new KMC model of particle evolution in oxidizing conditions based on the cluster expansion (details are provided in section 3.4 of the Supporting Information). We performed KMC simulations on nearly octahedral PtNi and Mo−PtNi particles with random initial atomic orders and initial compositions ($Pt_{4495}Ni_{1680}$ and $Pt_{4323}Ni_{1766}Mo_{86}$ with edge lengths of approximately 5.5 nm, Figure 3) matching those of the preactivated NPs (Figure S1). To account for the large difference between the overall composition (Ni% = 27.2, Table 1) and near-surface composition (Ni% = 46.6, XPS in Table S1) for the PtNi particle, we initialize the particle with randomly distributed Ni with a composition of 46.6% Ni on the surface and 20.4% Ni in deeper layers, leading to the overall composition of 27.2% Ni. The Ni distribution in the Mo−PtNi particle is similarly initialized based on the XPS near-surface composition (Table S1), and we start with Mo atoms distributed on edge/vertex sites to be consistent with the previous results that Mo is preferentially located at the low-coordinated sites.[3,17]

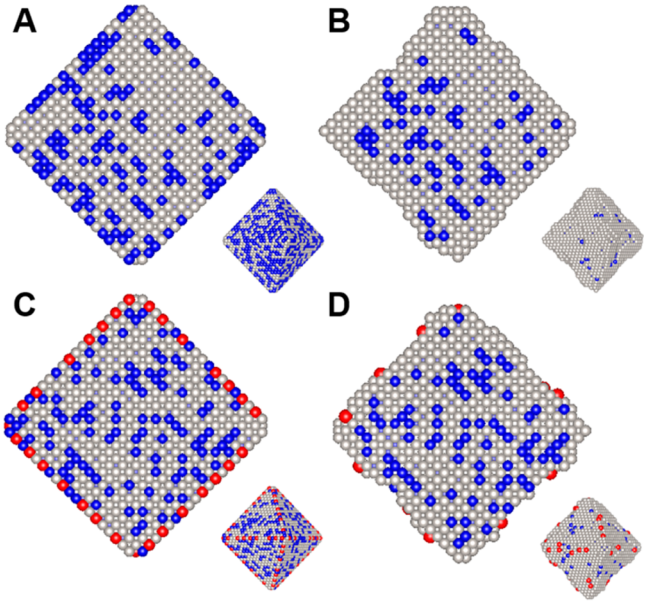

Figure 3. Middle cross-section of a PtNi particle before (A, with composition of $Pt_{4495}Ni_{1680}$) and after (B, with composition of $Pt_{4495}Ni_{895}$), and a Mo−PtNi particle before (C, with composition of $Pt_{4323}Ni_{1766}Mo_{86}$) and after (D, with composition of $Pt_{4323}Ni_{1289}Mo_{43}$) evolution under KMC simulations at a temperature of 27 °C (300 K). The insets at the bottom right show snapshots of the particles. The snapshots were taken when Ni composition reached the experimental compositions after activation for a PtNi particle in Table 1 (gray, blue, and red spheres represent Pt, Ni, and Mo atoms, respectively).

We stopped the KMC simulation in PtNi when the Ni composition reached the experimental composition after activation (16.6% Ni, Table 1). The resultant shape and site-specific Pt/Ni occupancies after Ni dissolution are shown in Figure 3. Most Ni atoms in the first and second layers dissolve to form a two-layer surface Pt-rich structure (Figure 3B), and the Pt/Ni sites deeper than the second layer are kinetically trapped in a disordered structure (Figure 3A,B). After approximately the same amount of simulated time, there was considerably less Ni loss in the Mo−PtNi particle (Figure 3C,D). The Ni fraction at the end of the KMC run on the Mo−PtNi particle drops to 22.8%, close to the experimental value for activated particles (25.0% Ni, Table 1). Mo continues to prefer low-coordinated sites, migrating to edge sites and step sites on (111) facets. The surface Mo (Mo^{4+}/Mo^{6+}) displaces Ni on the surface of Mo−PtNi NPs and lowers the mobility of Pt atoms in the outermost layer,[17] which reduces the exposure of subsurface Ni to vacant surface sites. This leads to a more Ni-rich second layer (Ni% = 26.8, simulation value) and the overall greater Ni composition (Figure 3D). The computational results not only support the experimental observation of less Ni exposed on the surface of Mo−PtNi/C compared to PtNi/C but also suggest that subsurface Ni is protected against acid dissolution by the presence of surface-doped Mo oxides.

Our DFT calculations on a prototypical particle estimate that MoO_3 (or MoO_2) withdraws *d*-band electrons from nearby Pt atoms (Figure S20J,K) and stabilizes them against dissolution by about 100 meV (details are provided in section 3.6 of the Supporting Information). Similarly, oxygenated adsorbates such as HO*/O* (* represents surface catalytic sites) that withdraw electrons from low-coordinated Pt sites have been found to stabilize these sites against dissolution.[17] However, the desorption of oxygenated adsorbates upon voltage cycling destabilizes the low-coordinated Pt sites, which can lead to dissolution and/or shape loss.[13,14] Unlike HO or O adsorbates, our calculations (Figure S18) and experiments (Figure 1B) indicate that Mo oxides (Mo^{4+}/Mo^{6+}) are present within the entire fuel cell operating potential range in acidic media and therefore are able to stabilize nearby low-coordinated Pt sites throughout electrochemical cycling, especially considering that low-coordinated Pt sites preferentially bind metal oxide dopants as nucleation centers.[35]

The electron transfer from Pt to Mo oxides indicated by our calculations was further investigated by the *in situ* XAS. The white line intensity of the Pt L_3-XANES arises from the electron transition from the 2p orbital to the vacant 5d-orbital and increases with increasing d-band vacancy.[36] Therefore, the lower white line intensity of the Pt XANES collected at 0.54 V (double layer region) of PtNi/C compared to that of Pt/C (Figure 4A) indicates decreased d-band vacancy of Pt. However, the white line intensity of the *in situ* Ni K-XANES of PtNi/C is higher than that of the Ni foil (Figure 4B), indicating increased d-band vacancy of Ni. These results indicates the electron donation from Ni to Pt, which has been observed in our calculations (Table S9) and demonstrated on

DOI: 10.1021/acs.nanolett.7b04007
Nano Lett. 2018, 18, 798−804

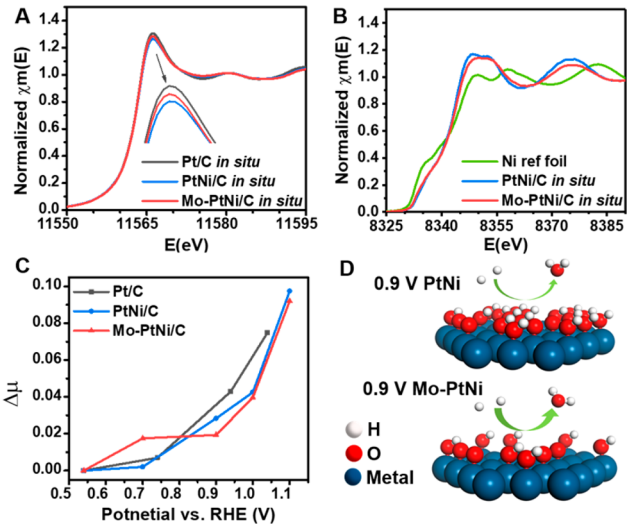

Figure 4. *In situ* Pt L_3-edge (A) and Ni K-edge (B) XANES spectra of PtNi/C, Mo−PtNi/C, and/or Pt/C catalysts collected on the electrodes at 0.54 V in O_2-purged 0.1 M $HClO_4$. (C) Potential-dependent changes in Pt L_3-edge absorption peaks: $\Delta\mu = \mu(V) - \mu(0.54\ V)$. (D) Brief sketch of O*/HO* adsorption on catalyst surface and correlated ORR performance at 0.9 V.

Pt_xNi_{1-x} single crystals using XAS,[37] and also agrees with the smaller electronegativity of Ni (1.91) compared to that of Pt (2.28). On average, the Ni in Mo−PtNi/C has fewer Pt neighbors (N_{NiPt} = 5.6 ± 0.8) than in PtNi/C (N_{NiPt} = 8.0 ± 0.8) due to the higher Ni concentration in Mo−PtNi/C. As a result, the Ni in Mo−PtNi/C has lower white line intensity (or more d-electrons) than that of PtNi/C owing to less electron acceptors (Figure 4B). Likewise, the Pt in Mo−PtNi/C at 0.54 V is expected to have lower white line intensity than PtNi/C due to lower d-band vacancy because of more electron-donating Ni neighbors. However, the Pt white line intensity of Mo−PtNi/C is higher than that of PtNi/C (Figure 4A). This result points to electron transfer from Pt to Mo oxides. This electron transfer direction is driven by the inherent tendency of electron donation from Pt with paired d-electrons to Mo cations with relatively empty d-orbitals[38] or to the oxygen in the oxides. Both trends have been previously confirmed on metal clusters supported on metal oxide (MMO) systems in which it has been observed that the metal oxide support stabilizes small Pt clusters enriched with low-coordinated Pt sites against dissolution.[39,40]

The experimental and computational results obtained thus far reveal that the Mo surface dopant stabilizes the desired $Pt_3Ni(111)$[1]-like near-surface structure in acidic operating conditions by enriching and stabilizing the subsurface Ni and by stabilizing the octahedral shape enriched with (111) facets. In addition, the surface Mo oxides may facilitate the ORR by modifying the coordination environments of Pt atoms on the surface. Figure 4C summarizes the derived $\Delta\mu$ amplitude ($|\Delta\mu|$) as a function of the applied potential wherein the $\Delta\mu$ signal was obtained by subtracting the Pt L_3 XANES collected at 0.54 V (in the double layer region relatively free of H and O adsorbates) from that collected at elevated potentials. The $\Delta\mu$ amplitude therefore reflects the relative oxygen coverage (original XANES spectra are provided in Figure S12).[31,41] The $|\Delta\mu|$ of Pt/C and PtNi/C increase monotonically with potential as seen previously;[31,41] whereas the Mo−PtNi shows a significantly different potential-dependent oxygen coverage trend (Figure 4C). Specifically, the $|\Delta\mu|$ of Mo−PtNi increases sharply when the potential was increased from 0.54 to 0.7 V, and then remains unchanged until 0.9 V (Figure 4C). As a result, the $|\Delta\mu|$ of Mo−PtNi/C is higher than that of Pt/C and PtNi/C at 0.7 V, but lower at 0.9 V (Figure 4C).

Increasing the thickness of the platinum shell around a Pt_3Ni nanoparticle increases the strength of the Pt−O bond while decreasing catalytic activity,[42] suggesting the activated PtNi/C NPs, which have a platinum shell that is about two layers thick, bind oxygen too strongly on average, and ORR activity on these particles is limited by the rate at which *OH is consumed. The relatively high coverage of *OH at 0.7 V on Mo−PtNi/C suggests that Mo increases the number of stable, low-coordinated Pt sites such as step sites, as these are the sites on which it is most facile for OH and related oxygen-containing species to adsorb.[3,43,44] The suppressed oxygen coverage of Mo−PtNi/C at 0.9 V indicates that the highly active (111) facet sites bind oxygen even more weakly on Mo−PtNi/C than they do on PtNi/C, further increasing their catalytic activity. This can be related to shorter Pt−Pt distance compared to that of Pt/C and PtNi/C, as the compressive-strain weakens the Pt−O binding energy.[31,32,45] In addition, our KMC simulations indicate that the Mo−PtNi/C NPs have a more Ni-rich second layer (Figure 3D), which should also result in lower oxygen adsorption energies than PtNi/C due to ligand effects.[45] The stabilization of Pt steps also produces overcoordinated Pt sites near the steps that are likely to bind OH relatively weakly and thus have high ORR activity.[44] The reduced adsorption energies for oxygen-containing species on the most catalytically active sites in activated Mo−PtNi/C are likely responsible for its superior catalytic activity.

In summary, combined experimental and computational results showed that the existence of surface Mo oxides on the Mo−PtNi/C octahedral NPs leads to increased concentrations of subsurface Ni and stabilizes undercoordinated Pt sites. This not only stabilizes the octahedral shape enriched with the (111) facet but also suppresses the acidic dissolution of the enriched subsurface Ni. As a consequence, the desired $Pt_3Ni(111)$-like near-surface structure is stabilized in acidic media throughout the entire fuel cell operating potential range against voltage cycling. In addition to these indirect promoting effects, the increased retention of Ni in the doped NPs directly improves the ORR kinetics by reducing the binding energies of oxygen-containing adsorbates. The elucidation of the promoting roles of surface transition metal dopants may pave the way for optimizing and stabilizing the surface morphologies of Pt-based NPs via surface doping strategy.

■ ASSOCIATED CONTENT

Supporting Information

The Supporting Information is available free of charge on the ACS Publications website at DOI: 10.1021/acs.nanolett.7b04007.

Experimental details of the synthesis, RDE testing, ex situ characterization, XAS measurements, EXAFS analysis, theoretical details of DFT calculations, the cluster expansion, and Monte Carlo simulations (PDF)

■ AUTHOR INFORMATION

Corresponding Authors

*E-mail: q.jia@neu.edu.
*E-mail: tmueller@jhu.edu.

DOI: 10.1021/acs.nanolett.7b04007
Nano Lett. 2018, 18, 798−804

*E-mail: yhuang@seas.ucla.edu.

ORCID

Qingying Jia: 0000-0002-4005-8894
Jingkun Li: 0000-0003-1699-3089
Zeyan Liu: 0000-0001-9237-7603
Xiangfeng Duan: 0000-0002-4321-6288
Sanjeev Mukerjee: 0000-0002-2980-7655
Yu Huang: 0000-0003-1793-0741

Author Contributions

Q.J., Z.Z., and L.C. contributed equally to this manuscript. The manuscript was written through contributions of all authors. Y.H. directed and conceived the research project. Q.J., J.L., S.G., V.D., E.S., K.A., and S.M. contributed to the *ex situ* and *in situ* XAS test. Z.Z., Z.L., M.L., and X.D. contributed to the materials preparation and *ex situ* characterizations. L.C. and T.M. contributed to computational studies.

Notes

The authors declare no competing financial interest.

■ ACKNOWLEDGMENTS

Y.H. acknowledges the support from the National Science Foundation through award no. DMR-1437263, and the Office of Naval Research under award N00014-15-1-2146. T.M. acknowledges support from the National Science Foundation under award no. DMR-1409765. Q.J. acknowledges the use of the Stanford Synchrotron Radiation Lightsource, SLAC National Accelerator Laboratory, supported by the U.S. Department of Energy (DOE), Office of Science, Office of Basic Energy Sciences under Contract No. DE-AC02-76SF00515. Use of Beamline 2-2 at SSRL and ISS 8-ID of the NSLS II was supported by the National Synchrotron Light Source (NSLS) II, Brookhaven National Laboratory, under U.S. DOE Contract No. DE-SC0012704. Computational resources were provided by the Center for Functional Nanomaterials at Brookhaven National Laboratory under grant 33818 and by the Maryland Advanced Research Computing Center (MARCC). Atomic-scale structural images were generated using VESTA.[46]

■ REFERENCES

(1) Stamenkovic, V. R.; Fowler, B.; Mun, B. S.; Wang, G.; Ross, P. N.; Lucas, C. A.; Marković, N. M. *Science* **2007**, *315* (5811), 493−497.
(2) Wagner, F. T.; Lakshmanan, B.; Mathias, M. F. *J. Phys. Chem. Lett.* **2010**, *1* (14), 2204−2219.
(3) Huang, X.; Zhao, Z.; Cao, L.; Chen, Y.; Zhu, E.; Lin, Z.; Li, M.; Yan, A.; Zettl, A.; Wang, Y. M. *Science* **2015**, *348* (6240), 1230−1234.
(4) Chen, C.; Kang, Y.; Huo, Z.; Zhu, Z.; Huang, W.; Xin, H. L.; Snyder, J. D.; Li, D.; Herron, J. A.; Mavrikakis, M. *Science* **2014**, *343* (6177), 1339−1343.
(5) Cui, C.; Gan, L.; Heggen, M.; Rudi, S.; Strasser, P. *Nat. Mater.* **2013**, *12* (8), 765−771.
(6) Niu, Z.; Becknell, N.; Yu, Y.; Kim, D.; Chen, C.; Kornienko, N.; Somorjai, G. A.; Yang, P. *Nat. Mater.* **2016**, *15*, 1188.
(7) Choi, S.-I.; Xie, S.; Shao, M.; Odell, J. H.; Lu, N.; Peng, H.-C.; Protsailo, L.; Guerrero, S.; Park, J.; Xia, X.; Wang, J.; Kim, M. J.; Xia, Y. *Nano Lett.* **2013**, *13* (7), 3420−3425.
(8) Huang, X.; Zhao, Z.; Chen, Y.; Zhu, E.; Li, M.; Duan, X.; Huang, Y. *Energy Environ. Sci.* **2014**, *7* (9), 2957−2962.
(9) Jia, Q.; Li, J.; Caldwell, K.; Ramaker, D. E.; Ziegelbauer, J. M.; Kukreja, R. S.; Kongkanand, A.; Mukerjee, S. *ACS Catal.* **2016**, *6* (2), 928−938.
(10) Han, B.; Carlton, C. E.; Kongkanand, A.; Kukreja, R. S.; Theobald, B. R.; Gan, L.; O'Malley, R.; Strasser, P.; Wagner, F. T.; Shao-Horn, Y. *Energy Environ. Sci.* **2015**, *8* (1), 258−266.
(11) Gan, L.; Cui, C.; Heggen, M.; Dionigi, F.; Rudi, S.; Strasser, P. *Science* **2014**, *346* (6216), 1502−1506.
(12) Stevens, D.; Mehrotra, R.; Sanderson, R.; Vernstrom, G.; Atanasoski, R.; Debe, M.; Dahn, J. *J. Electrochem. Soc.* **2011**, *158* (8), B905−B909.
(13) Greeley, J. *Electrochim. Acta* **2010**, *55* (20), 5545−5550.
(14) Wakisaka, M.; Asizawa, S.; Uchida, H.; Watanabe, M. *Phys. Chem. Chem. Phys.* **2010**, *12* (16), 4184−4190.
(15) Gasteiger, H. A.; Kocha, S. S.; Sompalli, B.; Wagner, F. T. *Appl. Catal., B* **2005**, *56* (1), 9−35.
(16) Hasché, F.; Oezaslan, M.; Strasser, P. *J. Electrochem. Soc.* **2011**, *159* (1), B24−B33.
(17) Cao, L.; Mueller, T. *Nano Lett.* **2016**, *16* (12), 7748−7754.
(18) Beermann, V.; Gocyla, M.; Willinger, E.; Rudi, S.; Heggen, M.; Dunin-Borkowski, R. E.; Willinger, M.-G.; Strasser, P. *Nano Lett.* **2016**, *16* (3), 1719−1725.
(19) Alonso-Vante, N.; Luo, Y.; Kirchhoff, B.; Fantauzzi, D.; Calvillo, L.; Estudillo-Wong, L. A.; Granozzi, G.; Jacob, T. *ChemSusChem* **2017**, DOI: 10.1002/cssc.201701822.
(20) Kohn, W.; Sham, L. J. *Phys. Rev.* **1965**, *140* (4A), A1133−A1138.
(21) Metropolis, N.; Rosenbluth, A. W.; Rosenbluth, M. N.; Teller, A. H.; Teller, E. *J. Chem. Phys.* **1953**, *21* (6), 1087−1092.
(22) Schulze, T. P. *J. Comput. Phys.* **2008**, *227* (4), 2455−2462.
(23) Serebrinsky, S. A. *Phys. Rev. E* **2011**, *83* (3), 037701.
(24) Sanchez, J. M.; Ducastelle, F.; Gratias, D. *Phys. A* **1984**, *128* (1), 334−350.
(25) Mueller, T.; Ceder, G. *Phys. Rev. B: Condens. Matter Mater. Phys.* **2009**, *80* (2), 024103.
(26) Mukerjee, S.; Urian, R. C. *Electrochim. Acta* **2002**, *47* (19), 3219−3231.
(27) Henke, B. L.; Gullikson, E. M.; Davis, J. C. *At. Data Nucl. Data Tables* **1993**, *54* (2), 181−342.
(28) Ahmadi, M.; Cui, C.; Mistry, H.; Strasser, P.; Roldan Cuenya, B. *ACS Nano* **2015**, *9* (11), 10686−10694.
(29) Becknell, N.; Kang, Y.; Chen, C.; Resasco, J.; Kornienko, N.; Guo, J.; Markovic, N. M.; Somorjai, G. A.; Stamenkovic, V. R.; Yang, P. *J. Am. Chem. Soc.* **2015**, *137* (50), 15817−15824.
(30) Ahmadi, M.; Behafarid, F.; Cui, C.; Strasser, P.; Cuenya, B. R. *ACS Nano* **2013**, *7* (10), 9195−9204.
(31) Jia, Q.; Liang, W.; Bates, M. K.; Mani, P.; Lee, W.; Mukerjee, S. *ACS Nano* **2015**, *9* (1), 387−400.
(32) Strasser, P.; Koh, S.; Anniyev, T.; Greeley, J.; More, K.; Yu, C.; Liu, Z.; Kaya, S.; Nordlund, D.; Ogasawara, H. *Nat. Chem.* **2010**, *2* (6), 454−460.
(33) Hercules, D. M.; Proctor, A.; Houalla, M. *Acc. Chem. Res.* **1994**, *27* (12), 387−393.
(34) Hwang, B.-J.; Sarma, L. S.; Chen, J.-M.; Chen, C.-H.; Shih, S.-C.; Wang, G.-R.; Liu, D.-G.; Lee, J.-F.; Tang, M.-T. *J. Am. Chem. Soc.* **2005**, *127* (31), 11140−11145.
(35) Subbaraman, R.; Tripkovic, D.; Strmcnik, D.; Chang, K.-C.; Uchimura, M.; Paulikas, A. P.; Stamenkovic, V.; Markovic, N. M. *Science* **2011**, *334* (6060), 1256−1260.
(36) Mukerjee, S.; Srinivasan, S.; Soriaga, M. P.; McBreen, J. *J. Electrochem. Soc.* **1995**, *142* (5), 1409−1422.
(37) Moraweck, B.; Renouprez, A.; Hlil, E.; Baudoing-Savois, R. *J. Phys. Chem.* **1993**, *97* (17), 4288−4292.
(38) Brewer, L. *Science* **1968**, *161* (3837), 115−122.
(39) Betta, R. A. D.; Boudart, M. *Proc. 5th Int. Congress on Catalysis*; Elsevier: North-Holland, Amsterdam, 1972; Vol. 2.
(40) Jia, Q.; Ghoshal, S.; Li, J.; Liang, W.; Meng, G.; Che, H.; Zhang, S.; Ma, Z.-F.; Mukerjee, S. *J. Am. Chem. Soc.* **2017**, *139* (23), 7893−7903.
(41) Li, J.; Alsudairi, A.; Ma, Z.-F.; Mukerjee, S.; Jia, Q. *J. Am. Chem. Soc.* **2017**, *139* (4), 1384−1387.

DOI: 10.1021/acs.nanolett.7b04007
Nano Lett. 2018, 18, 798−804

(42) Shao, M.; Odell, J. H.; Peles, A.; Su, D. *Chem. Commun.* **2014**, *50* (17), 2173−2176.
(43) Aarons, J.; Jones, L.; Varambhia, A.; MacArthur, K. E.; Ozkaya, D.; Sarwar, M.; Skylaris, C.-K.; Nellist, P. D. *Nano Lett.* **2017**, *17* (7), 4003−4012.
(44) Calle-Vallejo, F.; Pohl, M. D.; Reinisch, D.; Loffreda, D.; Sautet, P.; Bandarenka, A. S. *Chem. Sci.* **2017**, *8* (3), 2283−2289.
(45) Cao, L.; Mueller, T. *J. Phys. Chem. C* **2015**, *119* (31), 17735−17747.
(46) Momma, K.; Izumi, F. *J. Appl. Crystallogr.* **2008**, *41* (3), 653−658.

DOI: 10.1021/acs.nanolett.7b04007
Nano Lett. 2018, 18, 798−804